

# Multi-objective optimization of blank shape for deep drawing with variable blank holder force via sequential approximate optimization

Satoshi Kitayama<sup>1</sup> · Marina Saikyo<sup>2</sup> · Kiichiro Kawamoto<sup>3</sup> · Ken Yamamichi<sup>3</sup>

Received: 24 December 2013 / Revised: 1 May 2015 / Accepted: 19 June 2015 / Published online: 7 July 2015  
© Springer-Verlag Berlin Heidelberg 2015

**Abstract** Optimal blank shape minimizing earing in deep drawing has a direct influence on material saving as well as product quality. A number of methods for blank shape optimization have been previously proposed, most of which adopt a closed-loop type algorithm that requires a large number of simulation runs. Numerical simulation in sheet metal forming is so numerically intensive that it is preferable to find an optimal blank shape with a small number of simulation runs. This paper proposes a method for determining the optimal blank shape design in square cup deep drawing using sequential approximate optimization (SAO) with a radial basis function (RBF) network. Sheet metal forming is multi-objective in nature, and thus the blank shape design problem is formulated as a multi-objective design optimization. The aim is therefore to identify the pareto-frontier with a small number of simulation runs. The earing is minimized under tearing and wrinkling constraints with a variable blank holder force (VBHF), which varies through the punch stroke. Numerical results show that the disconnected pareto-frontier is well identified with a small number of simulation runs. The earing of the optimal blank shape with the VBHF is also drastically reduced, when compared to a reference blank shape. Based on the numerical results, the experiments using a servo press are carried out. Consequently, the validity of the proposed

approach is confirmed through the numerical and experimental results.

**Keywords** Blank Shape Optimization · Sequential Approximate Optimization · Multi-objective Optimization · Radial Basis Function network

## Abbreviations

BHF	Blank holder force
FEA	Finite element analysis
FLC	Forming limit curve
FLD	Forming limit diagram
GSE	Geometrical shape error
LHD	Latin hypercube design
LS-SVR	Least square support vector regression
MOO	Multi-objective optimization
RBF	Radial basis function
RSM	Response surface method
SAO	Sequential approximate optimization
SOO	Singe objective optimization
SPFC	Steel plate formability cold
SVR	Support vector regression
TSE	Target shape error

✉ Satoshi Kitayama  
kitayama-s@se.kanazawa-u.ac.jp

<sup>1</sup> Kanazawa University, Kakuma-machi, Kanazawa 920-1192, Japan

<sup>2</sup> Graduate School of Natural Science and Technology, Kanazawa University, Kakuma-machi, Kanazawa 920-1192, Japan

<sup>3</sup> Komatsu Industries Corp., 1-1, Ono-machi-shinmachi, Kanazawa 920-0225, Japan

## 1 Introduction

Sheet metal forming processes involve a complicated deformation that is affected by process parameters such as material properties, blank holder force (BHF), die geometry, blank shape, friction, and lubrication condition. Among these, the blank shape has a direct influence on the product quality. The desired product cannot be obtained with a small initial blank shape, while a large initial blank shape produces a large flange

part that is trimmed off as waste. Furthermore, a small BHF can lead to wrinkling while a large BHF results in tearing. Thus, it is important to find a suitable blank shape with an optimal BHF for the material saving and product quality. Traditionally, a trial-and-error method has been widely used to determine both the blank shape and BHF, but this is a time-consuming and difficult task. More recently, computer-aided engineering (CAE) based on finite element analysis (FEA) has been adopted as an alternative approach, and is recognized as one of the most powerful tools available (Gantar et al. 2002; Katayama et al. 2004). A number of different approaches have been proposed to determine the optimal blank shape in deep drawing, and these are mainly classified into two categories: the use of a closed-loop type algorithm, or those based on the response surface method (RSM).

In the closed-loop type algorithm approach, an algorithm is constructed based on FEA. In other words, a large number of simulation runs are required to determine the optimal blank shape. Park et al. proposed a method for determining optimal blank shape using the geometrical shape error (GSE) (Park et al. 1999), in which FEA is repeatedly carried out until the GSE value becomes very small. The distance between the target (the trimmed line) and the deformed shape along the deformation path of the nodes was used to determine the shape error. Shim et al. introduced the concept of shape sensitivity (Shim et al. 2000), which is calculated from the deformation path of nodes between the original blank and an offset blank. Kishor and Kumar considered the material flow during forming to predict the earing (Kishor and Kumar 2002). Pegada et al. also proposed an algorithm to determine the optimal blank shape (Pegada et al. 2002) in which, unlike in (Park et al. 1999), the shape error is simply calculated as the distance between the target and the deformed shape. In other words, the deformation path of the nodes is not taken into account by this method. The algorithm was repeated until the shape error was suitably reduced. Naceur et al. applied the evolutionary structural optimization (ESO) method to the blank shape optimization problem (Naceur et al. 2004), in that finite elements of the blank were simply eliminated under a volume constraint. Even though this method was based on FEA, the approach was completely different to that used by others (Park et al. 1999; Shim et al. 2000; Kishor and Kumar 2002; Pegada et al. 2002). The GSE is widely used for optimizing blank shape designs, and Wang et al. (2009); Vafaeesefat (2008, 2011), and Fazli and Arezoo (2012) adopted it for determining the optimal blank shape design in deep drawing. Oliveira et al. (Oliveira et al. 2009) indicated that GSE cannot determine whether the finite element nodes of the blank are inside or outside the target contour. They therefore proposed a target shape error (TSE), in order to quantify the magnitude of deviation of the flange contour from the required target contour. These GSE and TSE approaches are somewhat similar, but only TSE is able to take into

account the target contour. In a closed-loop type algorithm, since the finite element nodes of the blank are updated at each step, a large number of numerical simulation runs are required to obtain the optimal blank shape.

Sheet forming simulation is currently so numerically intensive that the use of RSM is a valid option (Bonte et al. 2008a). A quadratic polynomial is generally used for this, but the phenomena associated with sheet forming are inherently highly non-linear. Consequently, approximation using quadratic polynomial may result in poor quality. In order to obtain a more highly accurate response surface, the Kriging, the radial basis function (RBF) network, and the least square support vector regression (LS-SVR) using the Gaussian kernel should be used instead. In addition, the sequential approximate optimization (SAO) can be used to find a highly accurate global minimum with a small number of simulation runs, and has been recognized as one of the more important approaches available (Bonte et al. 2010). For the SAO of a single objective optimization (SOO) problem, the following procedure is performed:

- (STEP1) Initial sampling points are generated with latin hypercube design (LHD) and orthogonal array.
- (STEP2) Numerical simulation is carried out at the sampling points to obtain the response.
- (STEP3) Response surface is constructed, and the optimal solution for this is determined.
- (STEP4) The optimal solution and a few additional sampling points are used to improve the accuracy of response surface, and obtain a highly accurate global minimum.
- (STEP5) If the terminal criterion is satisfied, then the SAO algorithm will be terminated. Otherwise, the SAO algorithm is returned to STEP2.

The iteration of the above process allows a highly accurate global minimum to be found from a relatively small number of simulation runs. In the following, let us briefly review some papers on blank shape optimization using the SAO.

Hino et al. used the RSM for obtaining the optimal blank shape in deep drawing (Hino et al. 2006), in which earing, as defined by the amount of trimmed material, was minimized under two design constraints. Naceur et al. used a moving least square approximation to determine the optimal blank shape (Naceur et al. 2008), for which the risk of tearing/wrinkling was approximated using a quadratic polynomial, and 7 control points (nodes of the blank) were taken as the design variables. Similarly, Chamekh et al. approximated the GSE through an artificial neural network (back propagation) (Chamekh et al. 2010) using 7 control points as the design variables. Finally, Liu et al. optimized a polygonal blank shape by using support vector regression (SVR) (Liu et al. 2013), in

which the risk of tearing/wrinkling was approximated and 5 control points were taken as the design variables.

One of the advantages using closed-loop type algorithms is that a more accurate optimal blank shape can be obtained, as many nodes (control points) are used for determining the shape error. Unfortunately, this method also presents a number of issues:

- (P1) Only one objective function, such as the shape error, is essentially used in a closed-loop type algorithm. Sheet forming however is naturally multi-objective, but it is difficult to handle more than two objectives in a closed-loop type algorithm. It is therefore considered preferable to formulate a blank shape optimization problem as a multi-objective optimization (MOO) problem.
- (P2) A large number of simulation runs (function evaluations) are required to determine an optimal blank shape with a closed-loop type algorithm, when compared with the SAO approach. Although the SAO approach may not produce an optimal blank shape that is as accurate, it is far more important to obtain an approximate shape with a small number of simulation runs in order to reduce the required development time.
- (P3) The BHF plays an important role in product quality, but this has not been extensively discussed in blank shape optimization. In most cases, a constant BHF through the punch stroke is simply used. By adopting variable BHF (VBHF) approach, in which BHF varies throughout the punch stroke, improvements in the final product quality should be achievable (Chengzhi et al. 2005; Lin et al. 2007; Kitayama et al. 2010). Furthermore, the VBHF is not only useful for reducing the earing in deep drawing, but also for controlling the material flow into the die.

In order to resolve the aforementioned issues, this paper proposes a method for determining the optimal blank shape with the VBHF in deep drawing. The objective is to find out the optimal blank shape minimizing the earing under tearing/wrinkling constraints with the VBHF approach. In this paper, two objective functions are developed to evaluate the earing. The tearing/wrinkling is evaluated using the forming limit diagram (FLD) and are regarded as the design constraints. Unlike SOO, the aim of MOO is to identify a set of pareto-optimal solutions (or pareto-frontier in objective space); and in order to achieve this with a small number of simulation runs, the SAO approach using the RBF network has been adopted. In order to examine the validity of the proposed approach, the experiment using a servo press are also carried out.

In section 2 of this paper, a square cup FEA model and multi-objective design optimization problem are described. In section 3, the SAO approach is briefly described. Finally, numerical and experimental results are presented and

discussed in section 4. LS-DYNA was used to carry out the numerical simulation.

## 2 Blank shape optimization with variable blank holder force

### 2.1 Multi-objective optimization

Generally speaking, a multi-objective optimization (MOO) problem is formulated as follows (Miettinen 1998):

$$\left. \begin{array}{l} (f_1(\mathbf{x}), f_2(\mathbf{x}), \dots, f_K(\mathbf{x})) \rightarrow \min \\ x_i^L \leq x_i \leq x_i^U \quad i = 1, 2, \dots, n \\ g_j(\mathbf{x}) \leq 0 \quad j = 1, 2, \dots, ncon \end{array} \right\} \quad (1)$$

where  $f_i(\mathbf{x})$  is the  $i$ -th objective function to be minimized,  $K$  represents the number of objective functions,  $x_i$  denotes the  $i$ -th design variable,  $x_i^L$  and  $x_i^U$  are the lower and upper bounds of the  $i$ -th design variable,  $n$  represents the number of design variables,  $g_j(\mathbf{x})$  denotes the  $j$ -th design constraint, and  $ncon$  represents the number of design constraints.

### 2.2 Finite element analysis model

The FEA model used in this paper is shown in Fig. 1, in which the blank holder force is applied in the positive  $z$ -direction (Kitayama et al. 2010). All corner parts of the die denoted by the arrows in Fig. 1 are R8. The counter punch and die drop to the negative  $z$ -direction with a total stroke of 62 mm. At the bottom dead center, the counter punch, die, and blank holder all move upwards. The motions of these three items are shown in Fig. 2. The initial velocity is  $v_{\text{init}}=267$  mm/s, and the maximum velocity is  $v_{\text{max}}=359$  mm/s. The element type and the number of finite elements are shown in Table 1. The friction coefficient  $\mu$  of the interfaces (blank/blank holder, blank/punch, blank/die, and blank/counter punch) is set to 0.10. The initial blank size is 185 mm  $\times$  185 mm, and the initial thickness is 1.20 mm. Considering the symmetry, one-quarter model is used for the numerical simulation as shown in Fig. 1. Thus, an initial blank size of 92.5 mm  $\times$  92.5 mm is actually used in the numerical simulation. A Belyschko-Tsay shell element with seven integration points along the thickness direction is used for the shell mesh of the blank. The penalty coefficient for contact (blank/blank holder, blank/punch, blank/die, and blank/counter punch) is set to 0.10. The rigid element is employed to counter punch, die, blank holder, and punch, as listed in Table 1. In addition, Steel Plate Formability Cold (SPFC) 440 is selected as the test material. The material properties are listed in Table 2. The relationship of stress-strain is approximated by the database in LS-DYNA as follows:

$$\sigma = 793\epsilon^{0.189} \quad (2)$$

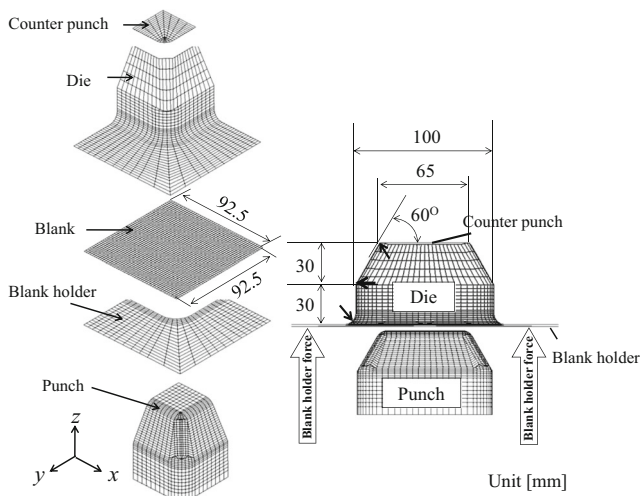


**Fig. 1** Finite element analysis model

The quarter-model deformation of the initial blank is shown in Fig. 3, in which the dashed line represents the target (trimmed) contour and the area above this contour is defined as earing. As shown in Fig. 3, the earing in this square cup deep drawing is generated in the  $x$ - $y$  plane. Ideally, the target contour should be set to the exact shape of the product denoted by the bold line. However, it is very difficult to set the exact shape as the ideal target contour in this deep drawing. As the result, the tolerance of 5 mm from the exact shape is considered and is set as the target contour. This approach is widely used for square cup deep drawing, and can be found in Refs. (Park et al. 1999; Shim et al. 2000; Naceur et al. 2004; Wang et al. 2009; Vafaeseefat 2008; Vafaeseefat 2011; Fazli and Arezoo 2012; Oliveira et al. 2009; Hino et al. 2006; Naceur et al. 2008; Liu et al. 2013).

**2.3 Design variables**

The blank shape is determined using the four design variables shown in Fig. 4, where one-quarter model of the formed product is depicted. The three nodes denoted by black squares are taken as the design variables for determining the blank shape.

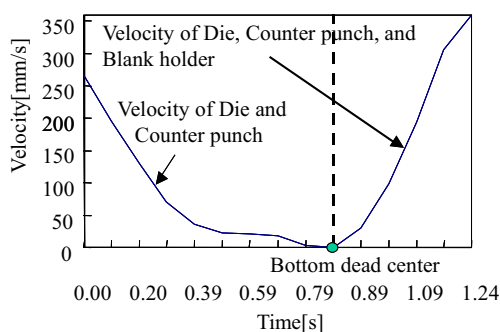


**Fig. 2** Motion of the die, blank holder, and counter punch

**Table 1** Element type and number of finite elements

	Element type	Number of finite elements
Counter punch	Rigid	120
Die	Rigid	924
Blank	Shell (Belytschko-Tsay)	2116
Blank holder	Rigid	432
Punch	Rigid	962

Nodes 1 and 3 move along the vertical and  $45^\circ$  line, respectively, while the movement of Node 2 depends on  $x_4$ . These nodes are connected by straight line as shown in Fig. 4, and the initial blank shape is then determined. VBHF is also taken into consideration to control the material flow into the die. For the VBHF, total stroke  $L_{max}$  is partitioned into  $M$  sub-stroke steps and the BHF of each sub-stroke is taken as the design variables. An illustrative example of these design variables is shown in Fig. 5, where it should be noted that the design variable for VBHF starts from  $x_5$ .

**2.4 Objective functions**

Minimization of earing is desirable for ensuring material saving and product quality. Let us explain how to evaluate the earing with Fig. 4, in which the dashed line represents the target (trimmed) contour. Both TSE and GSE use the node distance between the target and the deformed contour to evaluating the degree of earing. However, it is also possible to evaluate the earing directly using the area by the following procedure: First, the area above the target contour is evaluated as the first objective function  $f_1(x)$ , as shown in Fig. 4. Unfortunately, in this method, the area below the target contour cannot also be evaluated. Consequently, this area below the target contour is evaluated as the second objective function  $f_2(x)$ . As  $f_1(x)$  will be large with a large blank shape, while  $f_2(x)$  will be large with a small blank shape, a trade-off between these objectives can thus be observed.

There is another reason to consider the blank shape design problem as a MOO, as demonstrated by the illustrative examples of the initial and deformed blank shapes given in Fig. 6.

**Table 2** Material properties of SPFC440

Density: $\rho$ [kg/mm <sup>3</sup> ]	$7.84 \times 10^{-6}$
Young's modulus: $E$ [MPa]	$2.06 \times 10^5$
Poisson's ratio: $\nu$	0.3
Yield stress: $\sigma_Y$ [MPa]	353
Tensile strength: $\sigma_T$ [MPa]	479
Normal anisotropy coefficient: $r$	0.98
Strain hardening coefficient: $N$	0.189



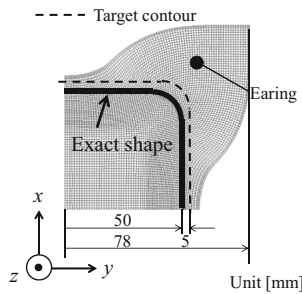


Fig. 3 Deformation of initial blank (quarter model)

These figures reveal that  $f_1(\mathbf{x})$  and  $f_2(\mathbf{x})$  depend on the initial blank shape, and it is difficult to determine an optimal blank shape while simultaneously minimizing both  $f_1(\mathbf{x})$  and  $f_2(\mathbf{x})$ . In addition, as described in section 2.3, the VBHF trajectory as well as the blank shape is determined in the proposed approach. If a single objective function is defined, only one VBHF trajectory could be obtained. However, this is not always true. Practically, there will be various VBHF trajectories for the successful forming. Under such conditions, a MOO is beneficial for determining both an optimal blank shape and VBHF trajectory. Thus, several VBHF trajectories could be obtained by formulating a multi-objective design optimization. A set of pareto-optimal solutions (or pareto-frontier) will be found, from which we can select a preferred solution. As discussed in section 1, the high cost of sheet forming simulation means that the pareto-frontier between  $f_1(\mathbf{x})$  and  $f_2(\mathbf{x})$  needs to be identified with a small number of simulation runs.

2.5 Constraints

Tearing and wrinkling are the major defects that typically occur in deep drawing, and are handled as the design constraints in this paper. The FLD is used to evaluate these defects, in which the strain states of all elements are plotted on a

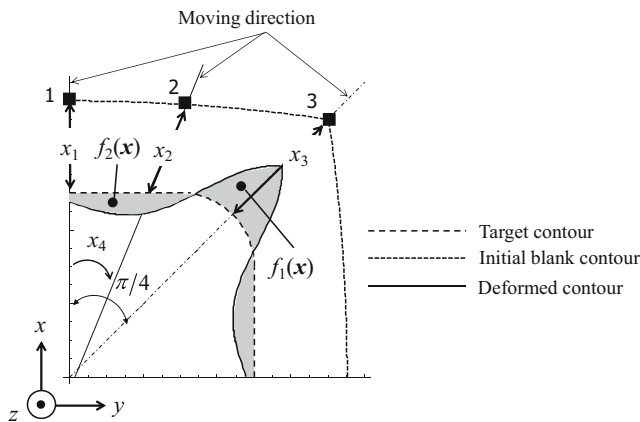


Fig. 4 Illustrative example for evaluating earing and design variables for blank shape

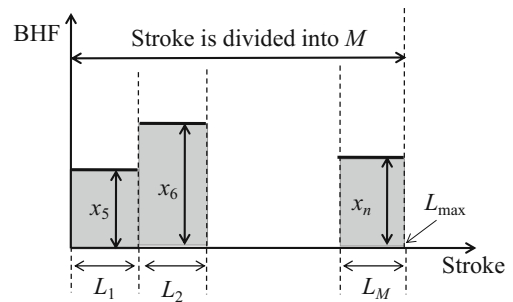


Fig. 5 Design variables for variable blank holder force

major-minor strain plane. In order to evaluate the degree of tearing and wrinkling, the strains in the formed element are analyzed and compared against the forming limit curve (FLC, as shown in Fig. 7). The following FLC was defined in the principal plane of logarithmic strains proposed by Hillman and Kubli (Hillmann and Kubli 1999).

$$\varepsilon_1 = \varphi_T(\varepsilon_2) \quad \varepsilon_1 = \varphi_W(\varepsilon_2) \tag{3}$$

where  $\varphi_T$  is the FLC that controls tearing, and  $\varphi_W$  is the FLC that controls wrinkling. It should be noted that both of these FLCs depend on the material; they are generally given as knots data in tables. Then, the following safety FLC is defined:

$$\left. \begin{aligned} \theta_T(\varepsilon_2) &= (1-s)\varphi_T(\varepsilon_2) \\ \theta_W(\varepsilon_2) &= (1+s)\varphi_W(\varepsilon_2) \end{aligned} \right\} \tag{4}$$

where  $s$  represents the safety tolerance, and is defined by the engineers (in this paper,  $s$  is set to 0.2). If an element comes to or lies above FLC, it is expected that a risk of

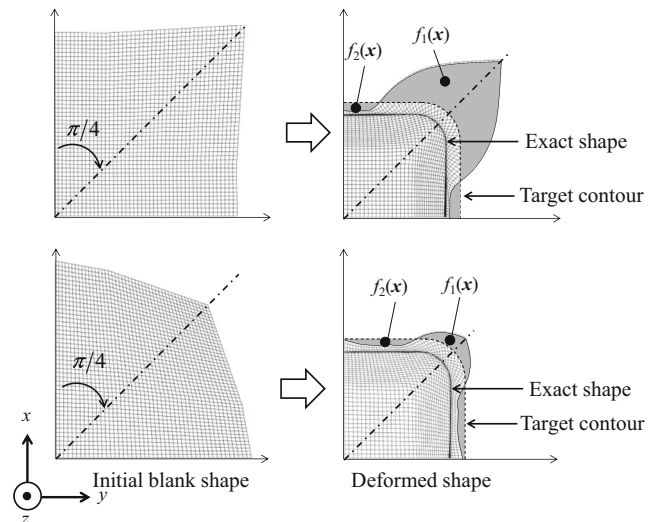


Fig. 6 Illustrative examples between initial blank shape and earing

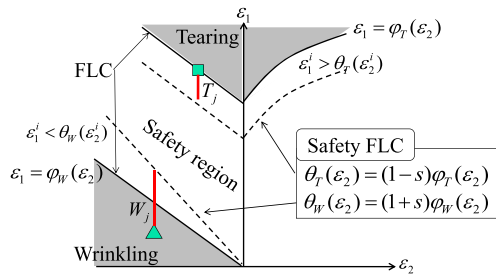


Fig. 7 Forming limit diagram for evaluating tearing and wrinkling

tearing can be observed. Similarly, a risk of wrinkling can be assumed if an element lies in the wrinkling region. Unlike previous studies (Wang et al. 2008a, b, 2010), the risk of both wrinkling and tearing were evaluated according to the following two constraints (Kitayama et al. 2012):

For tearing:

$$g_1(\mathbf{x}) = \left( \sum_{j=1}^{nelm} T_j \right)^{1/p} \tag{5}$$

where

$$T_j = \begin{cases} (\varepsilon_1^j - \theta_T(\varepsilon_2^j))^p & \varepsilon_1^j > \theta_T(\varepsilon_2^j) \\ T_j = 0 & \text{otherwise} \end{cases} \tag{6}$$

For wrinkling:

$$g_2(\mathbf{x}) = \left( \sum_{j=1}^{nelm} W_j \right)^{1/p} \tag{7}$$

where

$$W_j = \begin{cases} (\theta_W(\varepsilon_2^j) - \varepsilon_1^j)^p & \varepsilon_1^j < \theta_W(\varepsilon_2^j) \\ W_j = 0 & \text{otherwise} \end{cases} \tag{8}$$

Based on the literature (Wang et al. 2008a, b, 2010; Kitayama et al. 2012),  $p$  is set to 4. Also,  $nelm$  represents the number of finite elements of the blank.

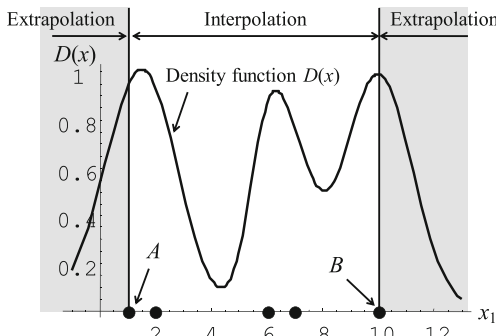


Fig. 8 Illustrative example of the density function in one dimension

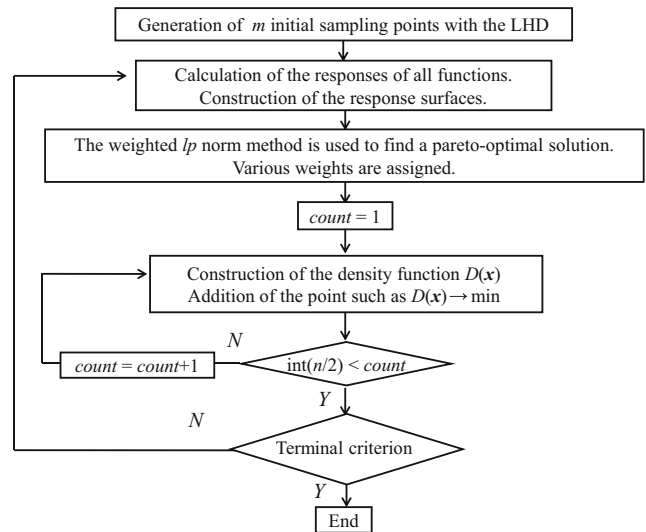


Fig. 9 Sequential approximate optimization algorithm for multi-objective optimization

### 3 Sequential approximate optimization using radial basis function network

SAO is now recognized as one of the most important optimization approaches in metal forming (Bonte et al. 2008b; Ingarao and Di Lorenzo 2010), and utilizes the repeated construction and optimization of response surface. This allows for a global minimum to be found from a relatively small number of function evaluations. Various SAO methods have been proposed, but this study adopts the RBF network.

#### 3.1 Radial basis function network

The RBF network is a three-layer feed-forward network. According to (Orr M.J.L.), given the training data expressed by  $\{x_j, y_j\}$  ( $j=1, 2, \dots, m$ ), where  $m$  represents the number of

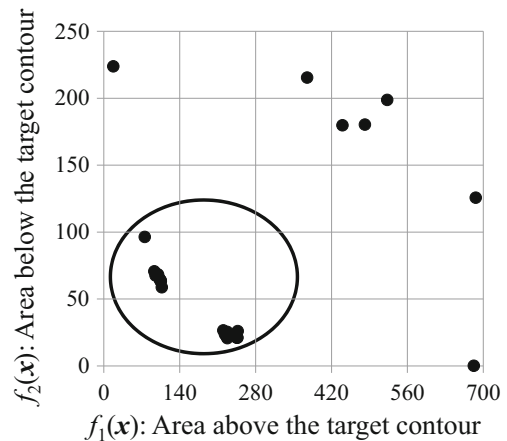
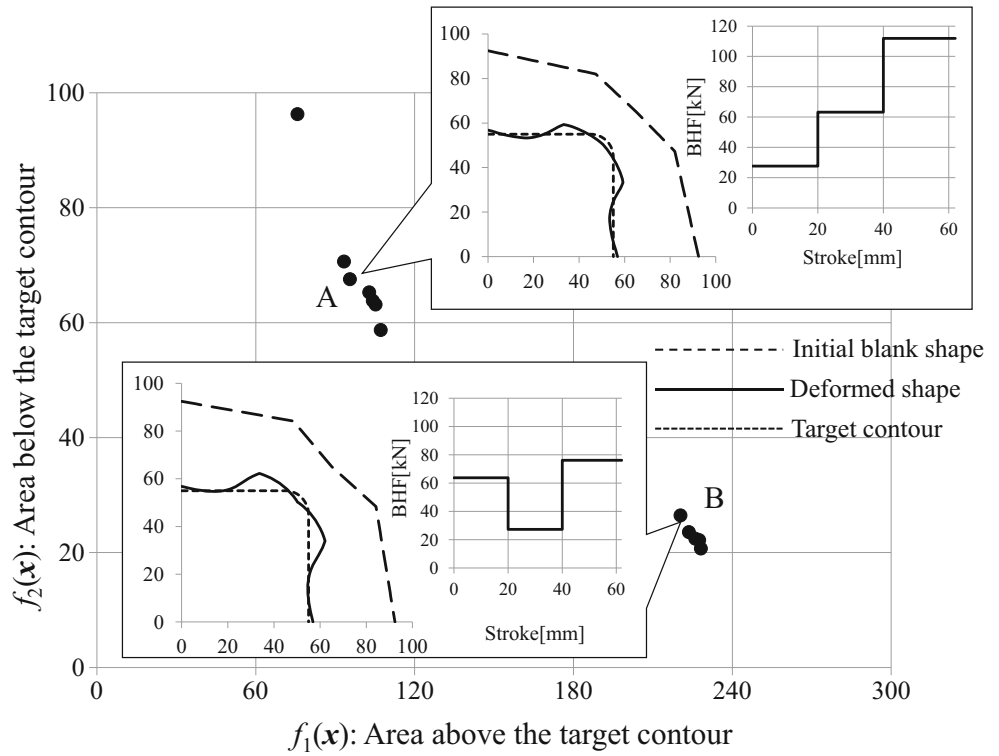


Fig. 10 All feasible sampling points in objective space

**Fig. 11** Pareto-frontier with an optimal blank shape and VBHF



sampling points, the output of the network  $\tilde{y}(\mathbf{x})$  (response surface) is given by

$$\tilde{y}(\mathbf{x}) = \sum_{j=1}^m w_j h_j(\mathbf{x}) \tag{9}$$

where  $h_j(\mathbf{x})$  is the  $j$ -th basis function, and  $w_j$  denotes the weight of the  $j$ -th basis function. The following Gaussian kernel is widely used as the basis function:

$$h_j(\mathbf{x}) = \exp\left(-\frac{(\mathbf{x}-\mathbf{x}_j)^T(\mathbf{x}-\mathbf{x}_j)}{r_j^2}\right) \tag{10}$$

where  $r_j$  is the width of the  $j$ -th basis function. The RBF network usually accomplishes learning by solving the following equation:

$$E = \sum_{j=1}^m (y_j - \tilde{y}(\mathbf{x}_j))^2 + \sum_{j=1}^m \lambda_j w_j^2 \rightarrow \min \tag{11}$$

where the second term is introduced for the purpose of regularization. It is also recommended that  $\lambda_j$  in (11) have a sufficiently small value (e.g.,  $\lambda_j = 1.0 \times 10^{-3}$ ). Thus, in the RBF network, the learning is equivalent to finding the weight vector  $\mathbf{w}$ . The necessary condition of (11) results in the following equation:

$$\mathbf{w} = (\mathbf{H}^T \mathbf{H} + \mathbf{\Lambda})^{-1} \mathbf{H}^T \mathbf{y} \tag{12}$$

where  $\mathbf{H}$ ,  $\mathbf{\Lambda}$ , and  $\mathbf{y}$  are given as follows:

$$\mathbf{H} = \begin{bmatrix} h_1(\mathbf{x}_1) & h_2(\mathbf{x}_1) & \cdots & h_m(\mathbf{x}_1) \\ h_1(\mathbf{x}_2) & h_2(\mathbf{x}_2) & \cdots & h_m(\mathbf{x}_2) \\ \vdots & \vdots & \ddots & \vdots \\ h_1(\mathbf{x}_m) & h_2(\mathbf{x}_m) & \cdots & h_m(\mathbf{x}_m) \end{bmatrix} \quad \mathbf{\Lambda} = \begin{bmatrix} \lambda_1 & 0 & \cdots & 0 \\ 0 & \lambda_2 & \cdots & 0 \\ \vdots & \vdots & \ddots & \vdots \\ 0 & 0 & 0 & \lambda_m \end{bmatrix} \tag{13}$$

$$\mathbf{y} = (y_1, y_2, \dots, y_m)^T \tag{14}$$

**Fig. 12** Minimum thickness at the corner region and thickness distribution

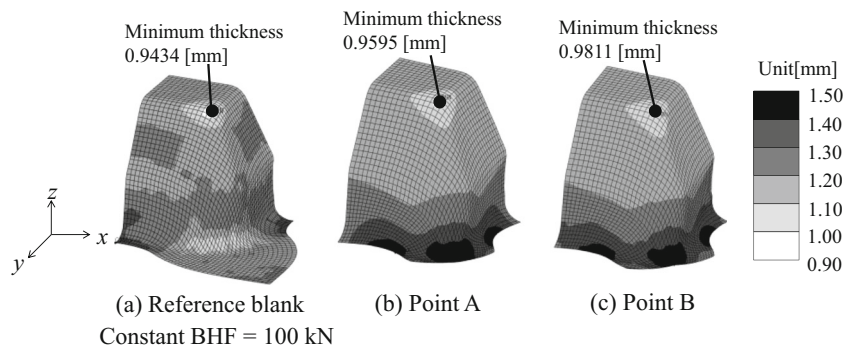


**Table 3** Comparison between reference and optimal blank shape

	Reference blank (constant BHF of 100 kN)	Optimal blank with VBHF		Improvement [%]	
		Point A	Point B	Point A	Point B
Area [mm <sup>2</sup> ]	8556	6633	6803	22.5	20.5
Earing [mm <sup>2</sup> ]	1989	104.3	226.1	94.8	88.6
Minimum thickness [mm]	0.9434	0.9595	0.9811	1.4	3.2

It is clear from (12) that the learning is equivalent to the matrix inversion  $(\mathbf{H}^T\mathbf{H}+\mathbf{A})^{-1}$ . Using the RBF network, it is easy to calculate the weight vector  $\mathbf{w}$ , because the additional learning is reduced to the incremental calculation of the matrix inversion (Nakayama et al. 2002).

In order to easily determine the width, the following simple estimate is proposed (Kitayama et al. 2011):

$$r_j = \frac{d_{j,\max}}{\sqrt{n}\sqrt{m-1}} \quad j = 1, 2, \dots, m \quad (15)$$

where  $r_j$  denotes the width of the  $j$ -th Gaussian kernel, and  $d_{j,\max}$  denotes the maximum distance between the  $j$ -th sampling point and the other sampling points. (15) is applied to each Gaussian kernel individually, and can deal with the non-uniform distribution of the sampling points. (15) can also be successfully applied to the classifier using the least square support vector machine (LS-SVM) and the RBF network (Kitayama and Yamazaki 2011).

### 3.2 Density function

One of the key issues for successful optimization in SAO is how to find an unexplored region. By adding new sampling points around an unexplored region, a global approximation can be successfully achieved. To resolve this issue, we have developed the density function with the RBF network (Kitayama et al. 2011). The basic concept of the density

function is simple. Local maxima are generated at the sampling points. As the result, local minima are generated around the unexplored region. To achieve this objective, every output  $\mathbf{y}$  of the RBF network is replaced with +1. A detailed procedure for constructing this density function is summarized as follows:

(D-STEP1) The vector  $\mathbf{y}^D=(1, 1, \dots, 1)_{m \times 1}^T$  is prepared at the sampling points.

(D-STEP2) The weight vector  $\mathbf{w}^D$  of the density function  $D(\mathbf{x})$  is calculated as:

$$\mathbf{w}^D = (\mathbf{H}^T\mathbf{H} + \mathbf{A})^{-1}\mathbf{H}^T\mathbf{y}^D \quad (16)$$

(D-STEP3) The density function  $D(\mathbf{x})$  is minimized to determine the unexplored region.

$$D(\mathbf{x}) = \sum_{j=1}^m w_j^D h_j(\mathbf{x}) \rightarrow \min \quad (17)$$

(D-STEP4) The point minimizing  $D(\mathbf{x})$  is taken as the new sampling point.

Figure 8 provides an illustration of this process in one dimension, the black dots representing the sampling points. Note that local minima are generated around the unexplored region. The RBF network is essentially the interpolation between sampling points; and thus points A and B in Fig. 8 represent the lower and upper bounds of the design variable  $x_1$  of the density function.

**Fig. 13** Comparison between initial and optimal blank shape

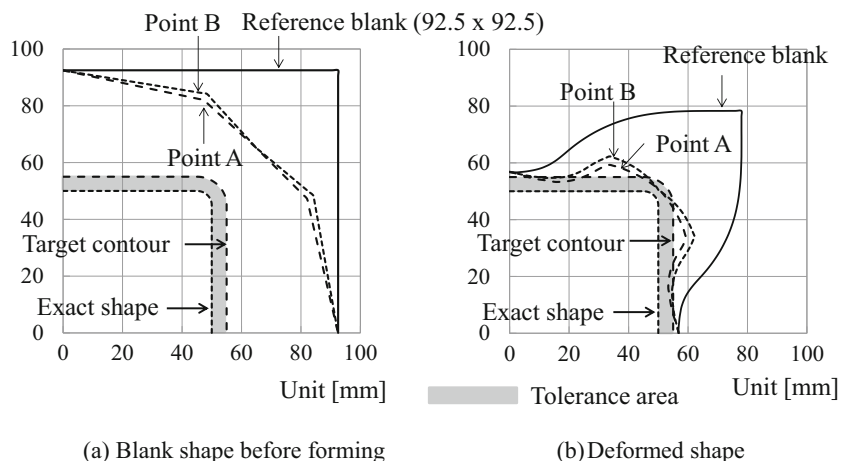
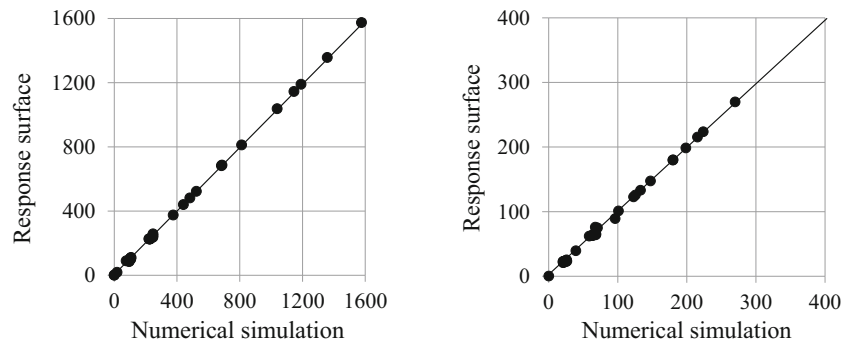




**Fig. 14** Accuracy of response surface



(a)  $f_1(x)$ : area above the target contour (b)  $f_2(x)$ : area below the target contour

### 3.3 Sequential approximate optimization for multi-objective optimization

The aim of SAO is to find a global minimum with a small number of sampling points (simulation runs), while the aim of MOO is to identify a set of pareto-optimal solutions. In this paper, the MOO problem described in section 2 is solved by using SAO; and consequently the aim is to identify a set of pareto-optimal solutions with a small number of sampling points. The flow can be summarized as follows:

- (STEP1) Initial sampling points are generated by the LHD.
- (STEP2) Numerical simulation is carried out, in which objective functions ( $f_i(\mathbf{x})(i=1,2,\dots,K)$ ) and constraints ( $g_j(\mathbf{x})(j=1,2,\dots,ncon)$ ) are numerically evaluated at all sampling points.
- (STEP3) All functions are approximated by the RBF network; wherein the approximated objective functions are denoted as  $\tilde{f}_i(\mathbf{x})(i=1,2,\dots,K)$ , and the approximated constraint functions are denoted as  $\tilde{g}_j(\mathbf{x})(j=1,2,\dots,ncon)$ .
- (STEP4) A pareto-optimal solution for the response surface is found using the weighted  $lp$  norm method formulated as follows (Chengzhi et al. 2005):

$$\left. \begin{aligned} & \left[ \sum_{i=1}^K \left( \alpha_i \tilde{f}_i(\mathbf{x}) \right)^p \right]^{1/p} \rightarrow \min \\ & \tilde{g}_j(\mathbf{x}) \leq 0 \quad j = 1, 2, \dots, ncon \end{aligned} \right\} \quad (18)$$

where  $\alpha_i(i=1,2,\dots,K)$  represents the weight of the  $i$ -th objective function, and  $p$  is the parameter (set to 4 in this paper). In order to obtain a set of pareto-optimal solutions, various weights are assigned.

- (STEP5) The density function is constructed and minimized, and the optimal solution of the density function is added as a new sampling point. This step is repeated till a terminal criterion is satisfied.

- (STEP6) If terminal criterion is satisfied, the SAO algorithm will be terminated. Otherwise, it is returned to STEP 2.

Figure 9 shows the proposed SAO algorithm for MOO, which offers the following advantages:

1. With the use of the weighted  $lp$  norm method, the MOO problem is transformed into a SOO problem; and thus we can apply the SAO for SOO to the MOO.
2. The weighted  $lp$  norm method is used to find a pareto-optimal solution, and the weight for each objective function should be assigned. Unlike the weighted sum, the weighted  $lp$  norm method can find a set of pareto-optimal solutions of the non-convex pareto-frontier with various weights (Chengzhi et al. 2005).
3. The density function is repeatedly constructed and minimized, as shown in Fig. 9, where the parameter *count* is introduced in this phase. This parameter controls the number of sampling points that can be obtained by the density function. Thus, in the proposed algorithm, the number of sampling points for the density function varies according to the number of design variables. If the parameter *count* is less than  $\text{int}(n/2)$ , this parameter is increased as  $\text{count} = \text{count} + 1$ . The terminal criterion in this stage is given by

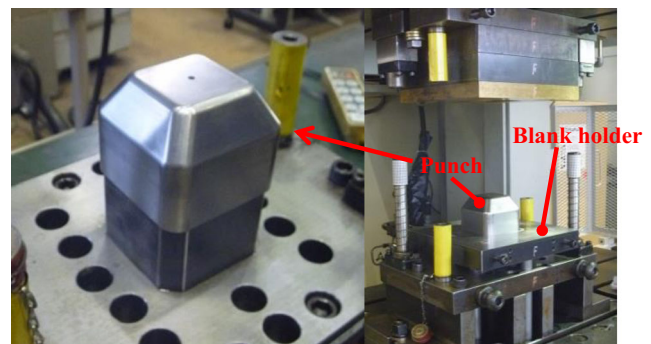
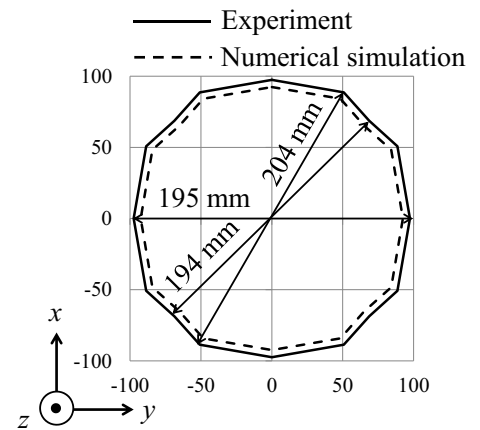
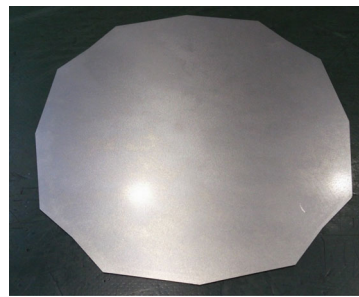


**Fig. 15** Punch and blank holder in the experiment

**Fig. 16** Blank shape used in the experiment



$\text{int}(n/2)$ , where  $\text{int}()$  denotes the rounding-off. It is expected that iterative use of the density function will yield a uniform distribution of sampling points. Furthermore, parts of disconnected pareto-optimal solutions may also be found by repeating this step.

**4 Numerical and experimental results**

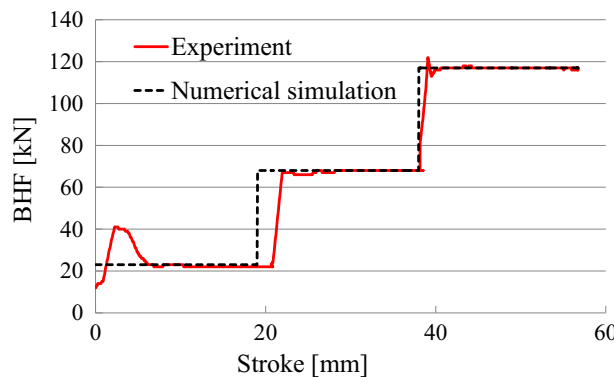
Numerical simulation was carried out to obtain the optimal blank shape and VBHF. In this paper, two objectives (the areas above/below the target contour) and two design constraints (wrinkling/tearing) are considered (therefore,  $K=2$  and  $n_{con}=2$ ). For the VBHF, the total stroke was divided into 3 ( $L_1, L_2$ , and  $L_3$ ). Then, the total number of design variables is 7. The lower and upper bounds of the design variables are defined as follows:

$$\left. \begin{aligned}
 &38 \leq x_1 \leq 42.5 [mm] \quad 33 \leq x_2 \leq 40 [mm] \quad 23 \leq x_3 \leq 62 [mm] \\
 &\pi/12 \leq x_4 \leq \pi/6 [rad] \\
 &20 \leq x_5 \leq 120 [kN] \quad \text{for } 0 \leq L_1 \leq 20 [mm] \\
 &20 \leq x_6 \leq 120 [kN] \quad \text{for } 20 \leq L_2 \leq 40 [mm] \\
 &20 \leq x_7 \leq 120 [kN] \quad \text{for } 40 \leq L_3 \leq 62 [mm]
 \end{aligned} \right\} \tag{19}$$

Fifteen initial sampling points are first generated with the LHD, and the pareto-frontier is identified. The error in the pareto-optimal solutions is adopted as the terminal criterion, which is set to 5.0 %. Various weights are assigned to the each objective function, and a total of 56 sampling points (simulation runs) are required to identify the pareto-frontier. All feasible sampling points in the objective space are shown in Fig. 10. In addition, an enlarged view of the enclosed region in Fig. 10 is shown in Fig. 11, in which the deformed shape using the optimal blank shape and VBHF at two representative points (A and B) is presented. From Figs. 10 and 11 it can be seen that the pareto-frontier is disconnected. Furthermore, we can also see that the optimal blank shape and the deformed shape are not qualitatively different, but the same is not true in the case of the optimal VBHF.

At point A, the initial BHF is low but gradually increases. This implies that the material readily flows into the die with the low BHF, but becomes hardened as the BHF increases. On the other hand, at point B, the material is hardened at the initial stage by the high BHF; with the lower BHF needing to be applied during the middle stage in order to prevent tearing. Finally, the material is again hardened by the high BHF at the final stage.

**Fig. 17** VBHF trajectory and product at point A



For optimization of both the blank shape and VBHF trajectory, an initial blank size of the quarter model ( $92.5 \times 92.5$  mm, which is giving the area of  $8556$  mm<sup>2</sup>) is used as the reference blank. The experiments using the reference blank have already been carried out in Ref. (Kitayama et al. 2010), in which a constant BHF and various VBHF trajectories were used for the successful sheet metal forming. The earing produced by this blank size is  $1989$  mm<sup>2</sup> (see Fig. 3), and the minimum thickness that is observed at the corner region shown in Fig. 12 is  $0.9434$  mm, from which it is also found that the thickness distribution is improved. Here, let us compare the following items at points A and B shown in Fig. 11: (1) the area of optimal blank before forming, (2) the earing associated with the optimal blank shape, and (3) the minimum thickness. Specific values are listed in Table 3, from which we can see that the optimal blank shape with the VBHF trajectory achieves an improvement over the reference blank in all aspects. Thus, the optimal blank shape with the optimal VBHF trajectory is beneficial for the material saving, and both the minimum thickness and the thickness distribution are also improved. Figure 13 shows a comparison between the reference and the optimal blank shape, from which the earing using the optimal blank shape can be seen to be drastically reduced. The results shown in Table 3 and Fig. 13 therefore confirm that the proposed approach is valid.

Finally, the accuracy of the response surfaces is shown in Fig. 14, from which it can be seen that a highly accurate response surface can also be obtained by this method.

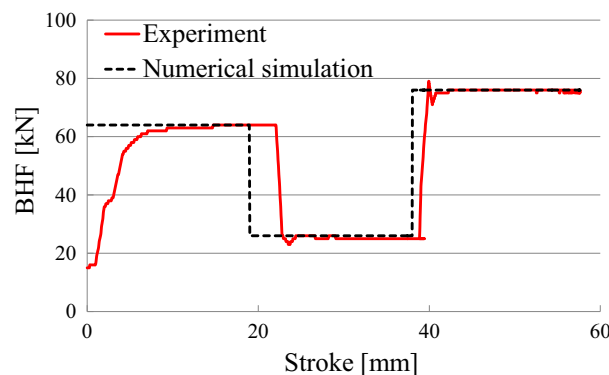
Based on the numerical results, the experiments using a servo press (H1F200, Komatsu Industry Corp.) are carried out. The photos of punch and blank holder are shown in Fig. 15. Points A and B shown in Fig. 11 is used for the experiments. It can be found from Fig. 13 that the optimal blank shape is not qualitatively different and the same blank shape is used in the experiments. In addition, an expert commented that the blank holder will be injured if the optimal blank obtained from the numerical result is directly used in the experiment. Based on his suggestion, the blank shape

considering the tolerance of  $5$  mm is used, which is shown in Fig. 16. The VBHF trajectory and the product through the experiments are shown in Figs. 17 and 18, respectively. In both figures, the solid line and the dashed line represent the VBHF trajectory in the experiments and in the numerical simulation, respectively. It is found from the experimental results that no tearing/wrinkling can be observed. The validity of the proposed approach is confirmed through the numerical and experimental results.

## 5 Concluding remarks

Blank shape in deep drawing has a direct influence on material saving and product quality, and it is important to determine the optimal blank shape. In this paper, the blank shape design is formulated as a multi-objective optimization in which two objective functions are considered: The first being the area above the target contour, while the other is the area below the target contour. Tearing and wrinkling are taken as the design constraints, and are evaluated using the forming limit diagram. In addition, variable blank holder force is adopted for improving the product quality. Thus, both the blank shape and the variable blank holder force trajectory are determined simultaneously in this paper. Sheet forming simulation is so numerically intensive that the sequential approximate optimization with the radial basis function network is adopted. The pareto-frontier is identified with a small number of simulation runs, and we can find that the pareto-frontier is disconnected. Compared against a reference blank shape, the earing produced using the optimal blank shape with the variable blank holder force is drastically reduced. The numerical result indicates that there are two kinds of VBHF trajectories for the successful sheet forming whereas the optimal blank is qualitatively same. Based on the numerical results, the experiments using servo press is carried out. No tearing/wrinkling can be observed through the experiments, and the validity of the proposed approach is then confirmed.

**Fig. 18** VBHF trajectory and product at point B



## References

- Bonte MHA, van den Boogaard AH, Huetink J (2008a) An optimization strategy for industrial metal forming processes –Modelling, screening and solving of optimization problems in metal forming. *Struct Multidiscip Optim* 35:571–586
- Bonte MHA, van den Boogaard AH, Huetink J (2008b) An optimization strategy for industrial metal forming processes. *Struct Multidiscip Optim* 35:571–586
- Bonte MHA, Fourment L, Do T, van den Boogaard AH, Huetink J (2010) Optimization of forging processes using finite element simulations – A comparison of sequential approximate optimization and other algorithms. *Struct Multidiscip Optim* 42:797–810
- Chamekh A, BenRhaïem S, Khaterchi H, BelHadjSalah H, Hambli R (2010) An optimization strategy based on a metamodel applied for the prediction of the initial blank shape in a deep drawing process. *Int J Adv Manuf Technol* 50:93–100
- Chengzhi S, Guanlong C, Zhongqin L (2005) Determining the optimum variable blank-holder forces using adaptive response surface methodology (ARSM). *Int J Adv Manuf Technol* 26:23–29
- Fazli A, Arezoo B (2012) A comparison of numerical iteration based algorithms in blank optimization. *Finite Elem Anal Des* 50:207–216
- Gantar G, Pepelnjak T, Kuzman K (2002) Optimization of sheet metal forming process by the use of numerical simulations. *J Mater Process Technol* 130–131:54–59
- Hillmann M, Kubli W (1999) Optimization of sheet metal forming processes using simulation programs, in: *Numisheet'99*. Beasnc, France 1:287–292
- Hino R, Yoshida F, Toropov VV (2006) Optimum blank design for sheet metal forming based on the interaction of high- and low-fidelity FE models. *Arch Appl Mech* 75(10):679–691
- Ingarao G, Di Lorenzo R (2010) Optimization methods for complex sheet metal stamping computer aided engineering. *Struct Multidiscip Optim* 42:459–480
- Katayama T, Nakamachi E, Nakamura Y, Ohta T, Morishita Y, Murase H (2004) Development of process design system for press forming – multi-objective optimization of intermediate die shape in transfer forming. *J Mater Process Technol* 155–156:1564–1570
- Kishor N, Kumar DR (2002) Optimization of initial blank shape to minimize earing in deep drawing using finite element method. *J Mater Process Technol* 130–131:20–30
- Kitayama S, Yamazaki K (2011) Simple estimate of the width in Gaussian kernel with adaptive scaling technique. *Appl Soft Comput* 11(8): 4726–4737
- Kitayama S, Hamano S, Yamazaki K, Kubo T, Nishikawa H, Kinoshita H (2010) A closed-loop type algorithm for determination of variable blank holder force trajectory and its application to square cup deep drawing. *Int J Adv Manuf Technol* 51:507–571
- Kitayama S, Arakawa M, Yamazaki K (2011) Sequential approximate optimization using radial basis function network for engineering optimization. *Optim Eng* 12(4):535–557
- Kitayama S, Kita K, Yamazaki K (2012) Optimization of variable blank holder force trajectory by sequential approximate optimization with RBF network. *J Adv Manuf Technol* 61(9–12):1067–1083
- Lin ZQ, Wang WR, Chen GL (2007) A new strategy to optimize variable blank holder force towards improving the forming limits of aluminum sheet metal forming. *J Mater Process Technol* 183:339–346
- Liu Y, Chen W, Ding L, Wang X (2013) Response surface methodology based on support vector regression for polygon blank shape optimization design. *Int J Adv Manuf Technol* 66:1397–1405
- Miettinen KM (1998) *Nonlinear Multiobjective Optimization*, Kluwer Academic Publishers
- Naceur H, Guo YQ, Batoz JL (2004) Blank optimization in sheet metal forming using an evolutionary algorithm. *J Mater Process Technol* 151:183–191
- Naceur H, Ben-Elechi S, Batoz JL, Knopf-Lenoir C (2008) Response surface methodology for the rapid design of aluminum sheet metal forming parameters. *Mater Des* 29:781–790
- Nakayama H, Arakawa M, Sasaki R (2002) Simulation-based optimization using computational intelligence. *Optim Eng* 3:201–214
- Oliveira MC, Padmanabhan R, Baptista AJ, Alves JL, Menezes LF (2009) Sensitivity study on some parameters in blank design. *Mater Des* 30:1223–1230
- Orr M.J.L., Introduction to Radial Basis Function Networks, <http://www.anc.ed.ac.uk/rbf/rbf.html> (On-line available)
- Park SH, Yoon JH, Yang DY, Kim YH (1999) Optimum blank design in sheet metal forming by the deformation path iteration method. *Int J Mech Sci* 41:1217–1232
- Pegada V, Chun Y, Santhanam S (2002) An algorithm for determining the optimal blank shape for the deep drawing of aluminum cups. *J Mater Process Technol* 125–126:743–750
- Shim H, Son K, Kim K (2000) Optimum blank shape design by sensitivity analysis. *J Mater Process Technol* 104:191–199
- Vafaeseefat A (2008) Optimum blank shape design in sheet metal forming by boundary projection method. *Int J Mater Form* 1:189–192
- Vafaeseefat A (2011) Finite element simulation for blank shape optimization in sheet metal forming. *Mater Manuf Process* 26:93–98
- Wang H, Li GY, Zhong ZH (2008a) Optimization of sheet metal forming processes by adaptive response surface based on intelligent sampling method. *J Mat Process Technol* 197:77–88
- Wang H, Li E, Li GY (2008b) Optimization of drawbead design in sheet metal forming based on intelligent sampling by using response surface methodology. *J Mat Process Technol* 206:45–55
- Wang J, Goel A, Yang F, Gau JT (2009) Blank optimization for sheet metal forming using multi-step finite element simulations. *Int J Adv Manuf Technol* 40:709–720
- Wang H, Li E, Li GY (2010) Parallel boundary and best neighbor searching sampling algorithm for drawbead design optimization in sheet metal forming. *Struct Multidiscip Optim* 41:309–324